



Supporting Online Material for
**Synchrony, Waves, and Spatial Hierarchies
in the Spread of Influenza**

Cécile Viboud,* Ottar N. Bjørnstad, David L. Smith,
Lone Simonsen, Mark A. Miller, Bryan T. Grenfell

*To whom correspondence should be addressed. E-mail: viboudc@mail.nih.gov

Published 30 March 2006 on *Science Express*
DOI: 10.1126/science.1125237

This PDF file includes:

Methods
SOM Text
Figs. S1 to S4
Tables S1 to S3
References

SUPPLEMENTARY ONLINE MATERIAL.

SYNCHRONY, WAVES AND SPATIAL HIERARCHIES IN THE SPREAD OF INFLUENZA

**Cécile Viboud^{1*}, Ottar N Bjørnstad^{1,2,3}, David L Smith¹, Lone Simonsen⁴, Mark A Miller¹,
Bryan T Grenfell^{1,3}.**

¹ Fogarty International Center, National Institutes of Health, Bethesda, MD 20892, USA; ² Department of Entomology, Pennsylvania State University, University Park, Pennsylvania 16802, USA; ³ Center for Infectious Disease Dynamics, Department of Biology, Pennsylvania State University, University Park, Pennsylvania 16802, USA; ⁴ National Institute of Allergy and Infectious Diseases, National Institutes of Health, Bethesda, MD 20818, USA

This supplementary material describes the data and methods in more detail, and presents additional analyses referred to in the main text. This material is organized as follows:

Data:

Epidemic data: p. 2-3 and Fig. S1

Geographic and movement data: p. 3-4 and Fig. S4

Methods:

Excess mortality model: p. 5

Timing, phase and synchrony analyses: p. 5-6

Statistical analysis of influenza spread, distance, and human movements: p. 7

Gravity model simulations: p. 7-9

Estimation of the effective reproduction ratio (R) and model fit: p. 9 and Table S2

Supplementary analyses:

Relationship between influenza-related mortality, morbidity and virus prevalence: p. 10-12 and Fig. S2, S3

Differences in virus subtype, disease spread and level of reporting: p. 12-14 and Table S3

Location of the initial epidemic focus in the US: p. 14-15

Epidemic synchrony and winter seasonality: p. 15-16 and Table S1

DATA

Epidemic data

- **Mortality data**

Assessment of the burden of influenza is not straightforward because the severe complications triggered by influenza infection, such as bacterial pneumonia, are often diagnosed after the infection has been cleared (1, 2). Many influenza-related deaths are therefore not coded as influenza but rather as underlying respiratory or chronic conditions. The traditional way to assess the mortality impact of influenza is to calculate excess mortality during influenza seasons, as the sum of deaths exceeding a baseline of expected deaths in the absence of influenza activity. Mortality from pneumonia and influenza (P&I) is considered a reliable indicator of the timing and relative severity of epidemics (1, 2).

Deaths from pneumonia and influenza (P&I) were obtained from the US vital statistics agency, the National Center for Health Statistics, for the period January 1st, 1972 to December 31st, 2002 (3). We used underlying codes of death 470-474 and 480-486 from the International Classification of Diseases (ICD) 8th revision, from 1972 to 1979, codes 480-487 from ICD-9 from 1979 to 1998, and codes J10.0-J18.9 from ICD-10 from 1999 to 2002 to select P&I deaths. P&I deaths were broken down by week (1,617 weeks in the study period) and by 49 administrative “states” in the US (48 Continental US states and the District of Columbia), based on the place of occurrence of deaths (Fig. 1). We excluded non-contiguous states (Hawaii and Alaska) since they consistently appeared as outliers in the analyses; probably because of weaker connections with the Continental US, potential importance of non-US areas for which we do not have data, and/or differences in climate and population. We standardized P&I deaths for changes in ICD revisions based on adjustment factors given by the National Center for Health Statistics (4). P&I death rates were then derived from annual population estimates from the US Census Bureau (5).

- Virus surveillance data

Unfortunately, virus surveillance data in the US are less extensive than mortality data; they are not available electronically at the weekly time scale for most years, nor are they available at the state level. Since virus surveillance does not give the within-season grain of the mortality data, we only use the virus data to identify predominant influenza subtype each season and confirm mortality patterns whenever possible.

To identify the predominant circulating subtypes for each influenza season, we reviewed annual Morbidity and Mortality Weekly Reports influenza summaries from the CDC (6-9). Fifty to 75 virology laboratories across the US participate to the CDC influenza virus surveillance each season from October through mid-May. We considered an influenza subtype dominant when it accounted for at least 70% of all isolates subtyped in that season (6). Of the 30 seasons studied, 1972/73 to 2001/02, A/H3N2 predominated in 17; A/H1N1, B, or a combination of these two subtypes dominated in the remaining 13 seasons.

In addition, we obtained a measure of overall influenza virus prevalence in the US each season by compiling the proportion of respiratory specimens sampled by the CDC that tested positive for influenza (7-10). Since this information became available in the winter 1976/77, the CDC has tested an average of 35,000 respiratory specimens per season. Since the number of specimens tested varied substantially across seasons, the proportion of influenza-positive specimen was considered a better indicator of virus prevalence than the number of positive specimens.

Geographic and movement data

- Geographic data

We obtained the geographical coordinates of the population centers in each state and county in continental US from the 2000 census (11). All geographical analyses used the population centers of US states or counties.

- Movement data

We compiled data on passenger air traffic across the US based on the “domestic

airline fares quarterly consumer report” from the US Department of Transportation, for the second quarter of 2000 (12). This report provides data on passenger flows between pairs of airports, based on 100% airline tickets issued (in airports with more than 10 passengers per day). To test for changes in geographical patterns of air traffic over time, we also examined a similar report for year 1990, the first year when this information became publicly available. Then, the datasets were aggregated by state to match the spatial resolution in the epidemiological data. The correlation coefficient between the 1990 and 2000 datasets was above 0.98 ($P < 0.0001$), suggesting that the geographical patterns did not change over the last decade, although the volume of passenger air traffic increased (by $\sim 40\%$). A limitation in the consumer report data is that individuals who transit an intermediate city are distinguished from persons who travel directly. For example, an individual flying from Miami to New York and connecting in Atlanta is counted as both a Miami-Atlanta and Atlanta-New York passenger. Hence this does not reflect the origin and final destination of each trip and the consumer data are probably biased towards large hubs in the airline network. To assess this bias, we investigated data on the origin and final destination of each trip for year 2000, available for 10% of all passengers (13). Note that the latter data may be less biased, but are also less precise, since they rely on a 10% sample of the actual trips taken. The correlation between the consumer data and the origin-destination data for 2000 was above 0.99 at the state level ($P < 0.0001$), suggesting that the bias towards large hubs was indeed minor. Hence subsequent analyses were performed with the more extensive airline consumer report from 2000.

We also compiled data on long-distance movements from the 1995 “American travel survey” from the US Bureau of Transportation Statistics (14). The Survey reported the cities of origin and destination for all long-distance trips taken by a sample of 80,000 households in the US (trips of more than 500 miles in total from the point of origin).

Moreover, we obtained data on flux-to-work from the US Census Bureau, which recorded the county of residence and county of workplace for all US residents in the 2000 Census (county-to-county worker flow file (15)).

METHODS

Excess mortality model

From the weekly time series of P&I deaths in each state for 1972-2002, we calculated *seasonal excess mortality* as the total mortality in excess of an epidemic baseline during winter months, separately for each state. To obtain a baseline for mortality in the absence of influenza, we applied a seasonal regression model adapted from the model developed by the CDC in 1963 (16) and recently refined (6, 17). We detail the algorithm briefly here. Before applying the seasonal model, we detrended the time series of weekly P&I mortality rates in each state by fitting a spline smooth function of time to the mortality for the summer weeks (June-August). Then we divided the original time series by the spline trend, to obtain detrended series with constant level of summer mortality. We then applied a seasonal regression model to the detrended series in each state, $Y_{t,i}$, excluding values for December-April, following:

$$Y_{t,i} = a_i + b_i * \cos(2\pi * t / 52.1667) + c_i * \sin(2\pi * t / 52.1667) + \varepsilon_{t,i}$$

where t is the index for week of death (from 1 to 1617), i the index for the state (from 1 to 51) and $\varepsilon_{t,i}$ is the error term.

Weekly excess mortality rates in each state were calculated as the observed minus predicted mortality rate during December-April. *Seasonal excess mortality* was estimated as the sum of weekly excess mortality, after back-adjusting for the time trend. All terms included in our model were statistically significant ($p < 0.0001$), but additional terms for time trends were not ($p > 0.05$). We conducted a sensitivity analysis by using monthly instead of weekly data to estimate seasonal excess mortality.

The total influenza mortality impact for the US (~ national epidemic size) was estimated by applying the above procedure to the aggregated time series of P&I deaths in the US.

Timing, phase and synchrony analyses

- Phase analysis (epidemic timing):

We conducted a phase analysis of the P&I mortality time series, following a methodology developed for the analysis of travelling waves in measles epidemics (18-

20). We reconstructed the weekly time series of phase angles in each state using wavelet reconstruction (20) to extract the major 1-year seasonal component (period 0.3 to 1.3 year) of the Morlet wavelet decomposition of P&I logged death rates.

- Spatial synchrony:

Analysis of spatial synchrony can provide insight into the similarities in epidemics occurring in neighboring locations (21). Synchrony of influenza epidemics in continental US was derived from pairwise (between-state) correlation in 3 different series: logged P&I mortality rates (a measure of the weekly amplitude and timing of epidemics, $n=1,617$ observations for each state), seasonal P&I excess mortality (a measure of amplitude aggregated over an influenza season, $n=30$ observations for each state) and P&I phase angles (a measure of weekly timing, $n=1,617$ observations for each state). The relation between synchrony and Euclidian distance was assessed using algorithms from the NCF library for R (22); in particular the spatial correlation function was estimated using the non-parametric spline covariance function and 500 bootstraps to generate 95% confidence bands (23).

- Analysis of the timing of the epidemic peak in each state

For all weekly P&I mortality time series, at the state and national level, the peak week was defined as the week with the maximum P&I death rate. Of the 30 epidemics studied, only 4 had two peaks, which were truly similar in magnitude and were mild epidemics. In this case, we always took the first peak; our purpose here was to consider the major epidemic – the center of mass of influenza in the season. Note that in the US and elsewhere, it is relatively common that a large A/H3N2 season ends in a period of low A/H1N1 or B activity; however in all these cases, surveillance reports a single winter peak of influenza transmission (see a discussion of this phenomenon in (24)). Results based on the timing of peak P&I excess mortality were confirmed by the wavelet phase analysis, which takes into account the entire epidemic cycle.

Statistical analysis of influenza spread, distance, and human movements

Influenza spread in continental US can be summarized by a 49×49 matrix, in which elements $a_{i,j}$ represent the “epidemic synchrony” between states i and j . We built two separate matrices representing epidemic synchrony, based on correlation in phases and $\log(\text{death rates})$. Then, we compared the epidemic matrices with the matrix of Euclidian distance between states, and 3 separate matrices of population movements based on air travels, long-distance trips and flux-to-work. Since the epidemic matrices were symmetric, the movement matrices were symmetrized by summing the movement between states $i \rightarrow j$ and $j \rightarrow i$. We estimated the association between the epidemic and distance/movement matrices using Spearman rank correlation and Mantel tests (25, 26). Since the elements of a distance matrix are not independent, the significance of the correlation coefficient was tested by permutation as described in (25, 26). We used partial Mantel tests to test the association between two matrices, while controlling for a third (25, 26).

In the geographical analyses, we use the administrative borders of states or counties to study the spread of influenza. This may not be exact since the natural unit of spatial spread is probably the city. Large cities usually comprise several counties, so that administrative borders should not affect county-level analyses. In contrast, administrative borders may have an impact on some of the state-level analysis; however only 5 of the 20 largest US cities are located on the border of 2 states (<http://www.census.gov/>). Further, using administrative borders may dilute the relationships between disease spread and transportation data (ie, bias towards the null), but this is unlikely to spuriously favor one transportation mode versus another.

Simulating influenza spread in the US using a gravity model fitted to workflow data

To explore the stochastic behavior of a patch-based SIR model with a gravity formulation for between-patch coupling, we let S , I , and R denote vectors of the number of susceptible, infected, and recovered individuals in the 49 continental US states. We let $\nu = 1/3.5$ denote the daily probability that an individual recovers, and βI the daily per-capita rate of infection from infectious individuals in-state. Here, β varies from state-to-state; it is a vector scaled such that the effective $R = \beta N / \nu$ is equal everywhere (as

consistent with estimates from data; see below), counting only within-state contacts (N is the vector of state population sizes). The per-capita rate of contact with infectious individuals from other states is given by γI , where γ represents between-patch coupling; γ is a scalar multiplied by the gravity matrix of movements which has zeros along the diagonal and off-diagonal elements based on the gravity model $\text{Pop}^{\tau_1} * \text{Pop}^{\tau_2} / \text{Distance}^{\rho}$, where the exponents τ_1 , τ_2 and ρ are estimated from the observed work movements (see main text and (15)). This introduces one free parameter to scale the amount of contact that occurs among individuals in different states, relative to individuals within states. Therefore, the expected number of contacts, per person per day, is $\beta (I + \gamma I)$, and the probability that an individual becomes infected is taken from the non-zero terms of a Poisson, $1 - e^{-\beta (I + \gamma I)}$. The stochastic dynamics are then described by the following spatially-extended chain-binomial system:

$$\begin{aligned} S_{t+1} &= S_t - W_t \\ I_{t+1} &= I_t + W_t - V_t \\ R_{t+1} &= R_t + V_t \\ W_t &= \text{binomial}(S_t, 1 - e^{-\beta (I + \gamma I)}) \\ V_t &= \text{binomial}(I_t, \nu). \end{aligned}$$

Here, W_t is the daily incidence (ie the number of new cases), and V_t is the number of new ‘recovereds’.

In simulations, the epidemic is initialized by infecting 5 individuals in a predetermined state; we chose to investigate an epidemic start in the most populous state, California, and for contrast, in the least populous state, Wyoming. After the first infection occurs in each state, we draw a multinomial to determine the source of the infection, from a normalized vector γI .

When the maximum element of the coupling matrix, γ , is less than approximately 10^{-5} , the epidemic tends to die out before spreading to other states. When the maximum element is larger than unity, the spread across the 49 states is almost instantaneous (< 4 days). In between these values, realistic patterns of spread are found, which match the observed level of synchrony in the empirical influenza data. In the simulations shown, we

set the maximum element of γ at 10^{-1} (see Table S2 for comparison of the duration of spread between observed and simulated epidemics). We note that the maximum ratio of any two elements off the main diagonal in γ is in the order 10^4 .

Calibrating the gravity model by estimating the effective R from the data

The effective reproduction ratio R is a central quantity in SEIR-type models. In the gravity model in particular, it is important for epidemic spread (higher R leads to faster spread). We estimated R from large observed epidemics, dominated by A/H3N2 viruses, and used the average estimate in our model, $R=1.35$ [95% confidence interval 1.10-1.60] (see in particular Figures 4 B-C). To estimate R, we used the regression method of Ferrari et al. (27), where the estimator is relatively robust to under-reporting of cases -- here, deaths are only a small proportion of all influenza cases occurring. We used a weighted regression with weights proportional to the number of deaths, as in (27).

We found no relation between the R estimates in each state and the state population density ($P=0.25$) or population size ($P=0.99$), indicating that the effective reproductive ratio must be quite homogeneous between states. Note also that this is in agreement with an earlier study of the 1918 pandemic examining the reproductive ratio in 45 US cities (28). This study found no correlation between R and population size and density (nor with latitude, longitude, age or gender distribution (28); see also an early analysis by Pearl (29)).

To evaluate the gravity model predictions, we compared the predicted and observed sequence of timings of onsets in 16 “States” (14 most populated states + the Dakotas + Montana-Wyoming). We chose to combine the Dakotas and Montana-Wyoming because of their geographical proximity, as well as to be able evaluate the model fit in less populated areas, while at the same time not being overwhelmed by observational errors. The gravity model showed good agreement in the overall duration of epidemics (Table S2) and also in the sequence of timings of onsets in general. For the 1999/00 epidemic for instance, which started out of California, the correlation between observed and predicted dates of onsets in the 16 “States” was 0.77.

SUPPLEMENTARY ANALYSES

Association between influenza virus prevalence, morbidity and mortality

- Mortality and epidemic timing

We checked that the weekly time series of P&I mortality were a good indicator of influenza epidemic timing. We compared the peak week in the P&I mortality data for the US with the peak week in the CDC's data on influenza virus prevalence, for each winter from 1979 to 2002 (the period when both data were available). We found a good agreement in timing between mortality and virus data, with high correlation (Spearman correlation coefficient = 0.83, $P < 0.01$) and a median difference in peak week of 1 week (range 0-4) (Fig. S2A).

- Mortality and virus prevalence

To check that our measure of influenza mortality impact could be used as a proxy for the level of influenza transmission in the community, we investigated the association between seasonal P&I excess mortality and the CDC's estimate of average virus prevalence each season. Although this estimate of average virus prevalence is a poor indicator of overall disease transmission (we return to this later), it is the only indicator available in the US. Influenza virus prevalence and mortality were highly correlated (Spearman correlation coefficient = 0.64, $P < 0.01$, Fig. S2B).

- Mortality and morbidity (UK)

Next we examined the relation between mortality and morbidity impact, as measured by the number of influenza-like-illnesses (clinical flu) monitored by general practitioners. Since there is no such measure of morbidity in the US, we investigated this relation from published data for the UK for the period 1987-99 (30). Influenza mortality and morbidity were strongly correlated (Spearman correlation coefficient = 0.88, $P < 0.01$, Fig. S2C).

- Mortality and hospitalizations

There are no data on overall influenza morbidity in the US, yet, there are data on hospitalizations, an indicator of severe morbidity. Previous work has shown strong correlation between influenza-related hospitalizations and mortality, even when each subtype is considered separately (see for instance (31)). We show this relationship in Fig.

S2D for the period 1989-2002, based on the hospitalizations data from the Agency for Healthcare Research and Quality (<http://www.ahrq.gov/>), which represents 16 states in the US and about half of the US population (correlation between hospitalization and mortality $\rho=0.97$, $P<0.01$).

- Relevance of various indicators of influenza activity

A literature search reveals that indicators of influenza virus prevalence, morbidity and mortality have been thoroughly compared in the UK (32-34). A strong agreement was reported between influenza-related mortality and influenza-like-illnesses monitored by sentinel physicians, both at the monthly and seasonal time scale (Spearman $\rho=0.99$ for seasonal impact, and Spearman $\rho =0.97$ for monthly data, all $P<0.01$, 1969/70 to 1980/81 (32, 33)). Encouragingly, these studies reveal both indicators to be consistent even during the two mildest A/H1N1 and B seasons of their study period. By contrast, virus prevalence was less correlated with mortality and influenza-like-illnesses, due to changes in laboratory surveillance of influenza over time (including changes in number of specimen sampled, case definition of patients, and isolation techniques). This explains the rather poor reliability of virus surveillance data for assessing the timing and impact of influenza epidemics, both in the UK and in the US. These findings were confirmed by a more recent analysis covering the 1980s and early 1990s, where a strong relationship was found between mortality and illnesses (correlation $\rho =0.92$, $P<0.001$), and a weaker relationship between mortality and virus prevalence ($\rho =0.60$, $P<0.001$; (34)). The strength of these relationships is very much in line with our own analysis of these indicators on the available US and UK data, as presented in Fig. S2B-C.

Another caveat in using influenza mortality and morbidity indicators as proxies for transmission relates to asymptomatic infections (infected but healthy individuals) and their role in disease transmission. The severity of influenza symptoms is directly related to the amount of viral shedding, for both influenza A and B (as suggested by several clinical studies, eg, (35, 36)), and hence to disease transmissibility. Therefore asymptomatic cases are probably not as important as symptomatic cases in the spread of influenza.

Taken together, these analyses and discussions indicate that influenza seasons

associated with higher mortality are also those with higher virus prevalence, and in turn higher transmission (modelled through a higher effective reproductive ratio R in our simulations). The relationship is probably stronger during A/H3N2 seasons. Overall, we conclude that influenza mortality can, with caution, be used as a proxy in the study of influenza spread.

Disease spread, virus subtypes and level of reporting

- Co-circulation of influenza subtypes

We have carefully considered the possibility that in seasons dominated by A/H1N1 and B viruses, the observed influenza mortality impact was due to a small number of co-circulating A/H3N2 viruses; but we found that this was not the case. There was no association between P&I excess mortality in A/H1N1-B seasons and the prevalence of A/H3N2 in the same seasons ($\rho=0.35$, $P=0.24$, $N=13$ seasons), suggesting a true quantitative relationship between prevalence of A/H1N1 and B infections and mortality.

As regards co-circulation of influenza (sub)types, it is worth noting that in the US, influenza seasons are neatly split into those strongly dominated by A/H3N2 and those where B and A/H1N1 dominate or co-dominate. Of the 29 influenza seasons fully characterized by the CDC from 1976/77 to 2004/2005, H3N2 dominated in 16 seasons, where by definition of “dominance” more than 70% of influenza specimens were identified as A/H3N2. In the remaining 13 seasons, B dominated in 6 (where it represented >70% of influenza isolates), A/H1N1 dominated in 2, and there was mixed circulation of A/H1N1 and B in 5 epidemics (~ 50%-50%) (6-9) (see also <http://www.cdc.gov/flu/weekly/fluactivity.htm> for recent years). Hence A/H1N1 and B epidemics could not be examined separately.

- Potential bias in subtype comparisons: role of level of reporting in estimates of disease spread

One might speculate that the observed subtype differences in disease spread (Fig 2F) stem from underlying differences in the level of reporting. In particular, consider a Null hypothesis where A/H1N1-B viruses are “milder” than A/H3N2 viruses in that they

are associated with a lower case fatality rate. Under this hypothesis, A/H1N1-B viruses might cause fewer deaths, even though the overall number of cases might be similar to that of A/H3N2 epidemics. We test this possibility by simulating A/H1N1-B epidemics under the Null hypothesis and comparing them with observed A/H1N1-B epidemics. To do so, we downsize observed H3N2 epidemics through binomial sampling (mirroring a lower sampling of deaths due to lower case fatality), so that the resulting simulated epidemics have a total death toll similar to that of observed A/H1N1-B epidemics. We consider 3 different scenarios for downsizing, by choosing 3 different H3N2 epidemics among the 17 observed between 1972 and 2002, which represent the observed range of A/H3N2 mortality impacts (~ min, max, and a median point, Table S3).

From the simulated downsized epidemics, we calculate the standard deviation (SD) between the date of the national peak and local peaks in each state -- which is the statistics used in Fig 2F. The SD of simulated A/H1N1-B epidemics is then compared with the SD of observed A/H1N1-B epidemics.

The results presented in Table S3 indicate that lower case fatality in A/H1N1 and B viruses is not biasing the comparison between subtypes, since the downsized A/H3N2 epidemics still reveal faster estimated spread than the observed A/H1N1-B epidemics. Note that the lower case fatality may still play, a role as shown by these simulations (Table S3), but it does not fully account for the observed differences in spread between A/H3N2 and A/H1N1-B epidemics.

- Perspectives related to subtypes comparisons, and pandemic versus epidemic spread

Of further interest is the comparison of the age pattern of infection between the various influenza subtypes – and resulting contact networks --, as A/H1N1-B viruses infect mostly children and young adults (37). Analysis of more refined incidence data should provide further insights into subtype differences in disease spread, beyond those driven by the overall level of transmission. Along the same line of thoughts, changes in the effective contact network of influenza may also occur during pandemics. It is worth noting that in previous pandemics, influenza attack rates in school-age children increased disproportionately as compared with those in adults (38), suggesting important

differences in the contact network of pandemic and inter-pandemic influenza. Predicting the spatiotemporal dynamics of such novel disease invasions is always a greater challenge because calibration against old epidemics is likely to be less accurate. On the other hand, pandemic viruses confront a much larger susceptible population, so that predicting their spread does not involve capturing the complex population profile of partial immunity encountered by inter-pandemic viruses (39)– although recycling of influenza antigens has been proposed for past pandemics (17, 40, 41).

Analysis of initial epidemic foci

We set out to identify the specific state(s) where each of the 30 epidemics started. Using the seasonal mortality baseline as described earlier, we defined the date of epidemic onset as the week when the observed P&I mortality first exceeded the baseline for two consecutive weeks. We repeated this analysis for each season and each state as well as for the aggregate US time series. We found that identifying the exact date of epidemic onset was difficult for smaller states where demographic noise was higher. To avoid confounding by noise, we restricted the analysis of epidemic onsets to the 10 most populous states in the US. These 10 states comprised locations in the East, West, North and South of the US and each of them had a population size between 8 and 30 millions (by decreasing population size, CA, TX, NY, FL, IL, PA, OH, MI, NJ, GA). Then we calculated the difference in weeks between the date of epidemic onset in 10 large states and the onset in the US time series. Next, we identified those states that had more frequent early onsets during the 30 influenza seasons under study.

California was the only state that was significantly early when compared with the national epidemic (average lead=1.0 week, $P < 0.0001$, Wilcoxon test). We also conducted a sensitivity analysis by using death rates specifically attributed to influenza instead of P&I death rates, a series believed to be more specific in terms of timing (see (6, 17), ICD-8 code 470-474; ICD-9 code 487; ICD-10 code J100-J118). The analysis of influenza-specific death codes also identified California as having early epidemics more often than other highly populated states.

Finally, we considered the hypothesis that epidemics started more often in California because it was the most populous state. To investigate this hypothesis, we

compared the timing of epidemic onsets in California with that in 3 large Eastern States combined (New York, New Jersey and Pennsylvania, where the combined population sizes and densities are larger than that in California). In this comparison, California had more frequent early onsets than the 3 Eastern states combined ($P < 0.01$). This result suggests that geographical factors may drive early epidemic activity in California, in addition to population factors. We think that international connections may play a role, and investigating international travels as potential drivers of the timing of epidemic onset is an area for future research.

Synchrony in the timing of influenza epidemics and seasonality

We found a high countrywide “global synchrony” in influenza epidemics across the US, especially with respect to the timing of epidemics (Fig. 2B). One might hypothesize that the high level of synchrony observed could be explained by the strong seasonality of influenza, known to drive epidemic timing in temperate areas of the world in general, and in the US in particular (1, 43). The alternative hypothesis is that not only seasonality, but also other factors, act together to synchronize epidemics.

To test the “Null” hypothesis that winter seasonality is the only synchronizing factor, we permute the 30 *influenza years* under study, independently for each state (here an influenza year runs from August to July), as described in (44). These permutations retain the common winter seasonality of influenza, but break the interdependence between states, thus removing the influence of other synchronizing factors. We then examine the synchrony among the permuted series, using the procedure described earlier and in references (21, 22). The statistics of interest here is the “global synchrony”, i.e. the average correlation across the US. 1,000 simulations give a null distribution of synchrony originating from seasonality alone.

We repeated this procedure for 3 types of epidemic time series: weekly logged death rates, weekly phases, and seasonal excess deaths. For all 3 types of epidemic series studied, the observed synchrony is much higher than that seen under permutation ($P < 0.001$, table S1), suggesting that observed epidemics are more synchronized than seasonality alone would predict. The simulations did, however, reveal that seasonality was responsible for part of the synchrony observed. Indeed for time series of weekly

death rates and phases, we found a positive and significant global synchrony in the data simulated under the Null hypothesis (Table S1). In contrast, for time series of seasonal excess deaths, no synchrony remained under the Null hypothesis, probably because of the aggregated time scale of this comparison.

This analysis supports the role of external factors superimposed on seasonality to drive the synchrony of influenza epidemics at the scale of the US. The analyses in the main text identify a dispersal force - movements to and from work - as one of these factors.

SUPPLEMENTARY REFERENCES

1. N. J. Cox, K. Subbarao, *Annu Rev Med* **51**, 407 (2000).
2. L. Simonsen, *Vaccine* **17 Suppl 1**, S3 (1999).
3. <http://www.cdc.gov/nchs/about/major/dvs/mortdata.htm>. (accessed Aug 3, 2005).
4. R. N. Anderson, A. M. Minino, D. L. Hoyert, H. M. Rosenberg, *Natl Vital Stat Rep* **49**, 1 (2001).
5. <http://www.census.gov/popest/estimates.php>. (accessed Aug 3, 2005).
6. L. Simonsen *et al.*, *Arch Intern Med* **165**, 265 (2005).
7. *MMWR Morb Mortal Wkly Rep* **49**, 375 (2000).
8. *MMWR Morb Mortal Wkly Rep* **50**, 466 (2001).
9. *MMWR Morb Mortal Wkly Rep* **51**, 503 (2002).
10. W. W. Thompson *et al.*, *Jama* **289**, 179 (2003).
11. <http://www.census.gov/geo/www/cenpop/cntpop2k.html>. (accessed Aug 3, 2005).
12. <http://ostpxweb.dot.gov/aviation/index.html>. (accessed Aug 3, 2005).
13. http://www.transtats.bts.gov/TableInfo.asp?Table_ID=289&DB_Short_Name=Origin%20and%20Destination%20Survey&Info_Only=0. (accessed Aug 3, 2005).
14. http://www.bts.gov/publications/1995_american_travel_survey/. (accessed Aug 3, 2005).
15. <http://www.census.gov/population/www/cen2000/commuting.html>. (accessed Aug 3, 2005).
16. R. Serfling, *Public Health Rep* **78**, 494 (1963).
17. C. Viboud, R. F. Grais, B. A. Lafont, M. A. Miller, L. Simonsen, *J Infect Dis* **192**, 233 (2005).
18. B. T. Grenfell, O. N. Bjornstad, J. Kappey, *Nature* **414**, 716 (2001).
19. O. N. Bjornstad, M. Peltonen, A. M. Liebhold, W. Baltensweiler, *Science* **298**, 1020 (2002).
20. C. Torrence, G. P. Compo, *Bull Am Meteorol Soc* **79**, 61 (1998).
21. A. M. Liebhold, W. D. Koenig, O. N. Bjornstad, *Annu Rev Ecol Evol Syst* **35**, 467 (2004).
22. <http://asi23.ent.psu.edu/onb1/>. (accessed Aug 3, 2005).

23. O. N. Bjornstad, W. Falck, *Environ Ecol Stat* **8**, 53 (2001).
24. A. Lavenu, A. J. Valleron, F. Carrat, *Virus Res* **103**, 101 (2004).
25. P. Legendre, L. Legendre, *Numerical ecology*. (Elsevier, Amsterdam, 1998).
26. <http://www.nceas.ucsb.edu/scicomp/Dloads/SpatialAnalysisEcologists/SpatialEcologyMantelTest.pdf>. (accessed Aug 3, 2005).
27. M. J. Ferrari, O. N. Bjornstad, A. P. Dobson, *Math Biosci* **198**, 14 (2005).
28. C. E. Mills, J. M. Robins, M. Lipsitch, *Nature* **432**, 904 (2004).
29. R. Pearl, *Public Health Rep.* **36**, 273 (1921).
30. D. M. Fleming, *Commun Dis Public Health* **3**, 32 (2000).
31. L. Simonsen, K. Fukuda, L. B. Schonberger, N. J. Cox, *J Infect Dis* **181**, 831 (2000).
32. H. E. Tillett, I. L. Spencer, *J Hyg (Lond)* **88**, 83 (1982).
33. H. E. Tillett, J. W. Smith, C. D. Gooch, *Int J Epidemiol* **12**, 344 (1983).
34. K. G. Nicholson, *Epidemiol Infect* **116**, 51 (1996).
35. C. B. Hall, R. G. Douglas, Jr., J. M. Geiman, M. P. Meagher, *J Infect Dis* **140**, 610 (1979).
36. K. G. Nicholson *et al.*, *Lancet* **355**, 1845 (2000).
37. W. P. Glezen, *Epidemiol Rev* **4**, 25 (1982).
38. S. L. Epstein, *J Infect Dis* **193**, 49 (2006).
39. N. M. Ferguson, A. P. Galvani, R. M. Bush, *Nature* **422**, 428 (2003).
40. D. R. Olson, L. Simonsen, P. J. Edelson, S. S. Morse, *Proc Natl Acad Sci U S A* **102**, 11059 (2005).
41. L. Simonsen, D. Olson, C. Viboud, M. Miller, “Pandemic Influenza and Mortality: Past Evidence and Projections for the Future” (Institute of Medicine, The National Academy of Sciences, 2004).
42. I. M. Longini, Jr., P. E. Fine, S. B. Thacker, *Am J Epidemiol* **123**, 383 (1986).
43. C. Viboud, W.J. Alonso, L. Simonsen, *PLoS Med* **3**, e89 (2006)
44. C. Viboud *et al.*, *Emerg Infect Dis* **10**, 32-9 (2004).

Table S1: Synchrony of influenza epidemics and winter seasonality. Observed global synchrony and simulated synchrony under the Null hypothesis that winter seasonality alone synchronizes epidemics.

Synchrony measure derived from P&I mortality data	Observed global synchrony Mean (95% CI)	Simulated global synchrony under Null hypothesis * Mean (95% CI)	P-value for difference between observed and Null distribution
Logged weekly death rates	0.54 (0.49-0.58)	0.32 (0.320-0.325)	<0.001
Weekly phases	0.79 (0.76-0.81)	0.682 (0.681-0.684)	<0.001
Seasonal excess deaths	0.57 (0.52-0.61)	0.00 (-0.01, +0.01)	<0.001

P&I, Pneumonia and Influenza; CI= Confidence Interval

* Null distribution of synchrony for 1,000 simulated time series where seasonality acts as the only synchronizing factor

Table S2: Comparison of the duration of influenza spread across the US in observed and simulated epidemics. Simulations use a gravity model based on workflows.

	Mean duration of spread across US states ^a	Maximum duration of spread (weeks) ^b
	Mean (range) in weeks ^c	Mean (range) in weeks ^c
Empirical data: 30 epidemics 1972-2002 ^d	5.2 (2.7 - 8.4)	6.9 (4.0 - 11.0)
Simulated epidemics (reproduction ratio=1.35)		
First case in California	4.7 (1.0 - 9.0)	6.0 (1.0 - 14.0)
First case in Wyoming	6.9 (1.0 - 14)	8.3 (1.0 - 18.0)
Simulated repeat of the 1968 pandemic (reproduction ratio=1.89 ^e)		
First case in California	2.2 (1.0 - 4.4)	3.6 (1.0 – 6.0)
First case in Wyoming	3.7 (1.0 – 7.5)	5.0 (1.0 – 8.0)

^a Average time between first case in the first epidemic state and first case in other states

^b Time between first case in the first epidemic state and first case in the last state

^c Mean and range across 30 epidemics (empirical data) or 1,000 runs of the gravity model (simulated data)

^d Time interval between peaks used as a proxy for time interval between first cases

^e Reproduction ratio for the 1968 pandemic as estimated in (42).

Table S3: Spread of epidemics in observed and simulated epidemics. Simulated “A/H1N1-B epidemics” are obtained by downsizing A/H3N2 epidemics through a binomial sampling, so as to obtain a mortality impact similar to observed H1N1-B epidemics. The spread statistics considered is the Standard Deviation (SD) of the differences in the timings of the local and national peaks (as in Figure 2F). The simulations rule out the hypothesis that the subtype difference is only due to differences in the level of reporting (ie case fatality).

Epidemics	Number of seasons	Mortality impact (median P&I excess death per 100,000)	Difference in peak dates* (Median SD in weeks)	Sampling probability for downsizing (simulated epidemics)
Observed H3N2	17	4.56	4.0	–
Observed H1N1-B	13	2.39	7.2	–
Simulated H1N1-B	100	2.39	4.8 (3.2-6.5)	0.41 ^a
	100	2.39	5.2 (3.2-6.8)	0.51 ^b
	100	2.39	5.6 (4.1-7.1)	0.71 ^c

* Difference between the week of the national peak and the week of the local peak

^a Simulations used the 1998/99 epidemic for downsizing

^b Simulations used the 1996/97 epidemic for downsizing

^c Simulations used the 2001/02 epidemic for downsizing

SUPPLEMENTARY FIGURES LEGEND

Supplementary Figure 1:

Time series of weekly excess deaths from pneumonia and influenza (P&I) in the US and each of the 49 Continental US states (District of Columbia included, Hawaii and Alaska excluded). A) National P&I excess deaths are shown per 100,000 population and have been normalized to have zero mean and unit variance. B) P&I excess deaths per 100,000 population are shown at the state level as a colour intensity plot; deaths have been normalized to have zero mean and unit variance **for each influenza year and each state**. The 49 states are arranged by decreasing population sizes (from top=California to bottom=Wyoming). Vertical bands in red correspond to synchronized epidemics, which occur in the most populated states or during larger epidemics, suggesting that synchrony increases with population size and epidemic size.

Supplementary Figure 2:

Relation between influenza mortality, morbidity, and virus prevalence, at the national scale. Dots represent the observed data (color-coded by dominant virus subtype) and the grey line is a linear fit.

A. Comparison of epidemic timing in weekly time series of Pneumonia and Influenza (P&I) mortality and the CDC's virus surveillance in the US. Epidemic timing is based on the week of maximum mortality (y-axis) and maximum virus prevalence (x-axis). Virus prevalence is defined as the proportion of respiratory samples positive for influenza.

B. Comparison of mortality impact and average virus prevalence during an influenza season in the US. National influenza mortality impact is estimated by seasonal P&I excess mortality rates (y-axis). Average virus prevalence is the cumulative proportion of respiratory samples positive for influenza over the season (x-axis).

C. Comparison of mortality and morbidity impact. Data for the UK taken from (30); influenza mortality impact is estimated by seasonal all-cause excess mortality rates (y-axis); morbidity impact is based on the number of visits for influenza-like-illnesses (clinical flu) recorded by general practitioners (x-axis), from 1987 to 1999.

D. Comparison of mortality and severe morbidity impact. National influenza

mortality impact is estimated by seasonal P&I excess mortality rates (y-axis). Severe morbidity is measured by excess P&I hospitalizations (data from the Agency for Healthcare Research and Quality), from 1989 to 2002 (x-axis).

Supplementary Figure 3:

Patterns of influenza spread and geographical distance (A) and prevalence of circulating viruses (B).

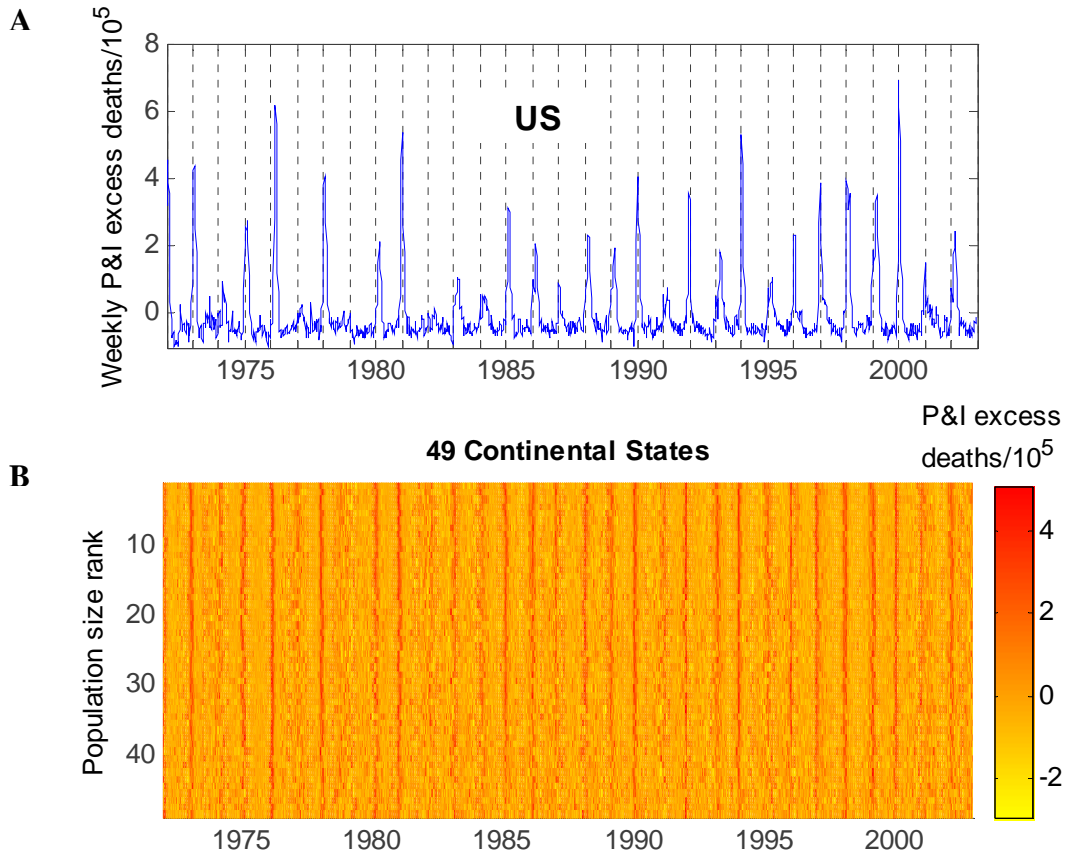
A) The synchrony in the trajectories of influenza epidemics (y-axis, measured as pair wise correlation in state-specific weekly P&I death rates) is plotted against the geographical distance between state population centers (x-axis). Synchrony function (black curve) and 95% confidence bands (red curves) are presented along with the global countrywide synchrony (horizontal red line).

B) Spread is measured by the standard deviation (SD) of the difference in the timing of epidemic peaks between national and local P&I mortality time series, in weeks (y-axis). National influenza virus prevalence is measured as the proportion of respiratory specimens tested positive for influenza across the US, 1976-2002 (26 seasons, CDC data, x-axis). Grey dashed line: linear fit: $R^2=0.24$, $P=0.01$. Because of gradual enhancements in the surveillance efforts of influenza by CDC, more specimens have tested positive over time ($P<0.0001$ for linear trend). However, repeating the analysis with a detrended proportion of influenza positive specimens gave the same relation between spread and virus prevalence.

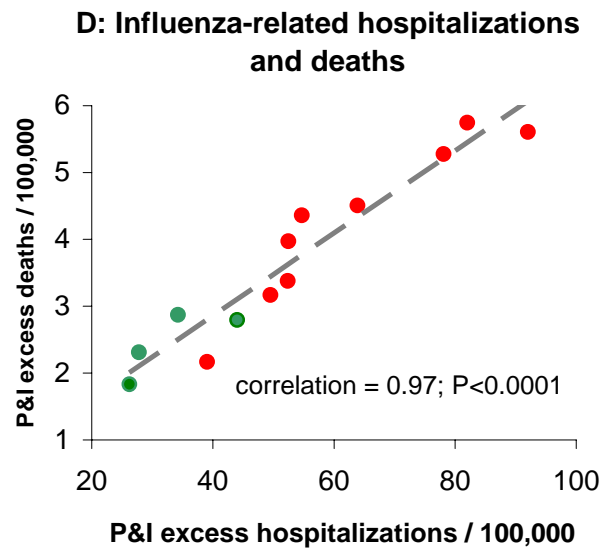
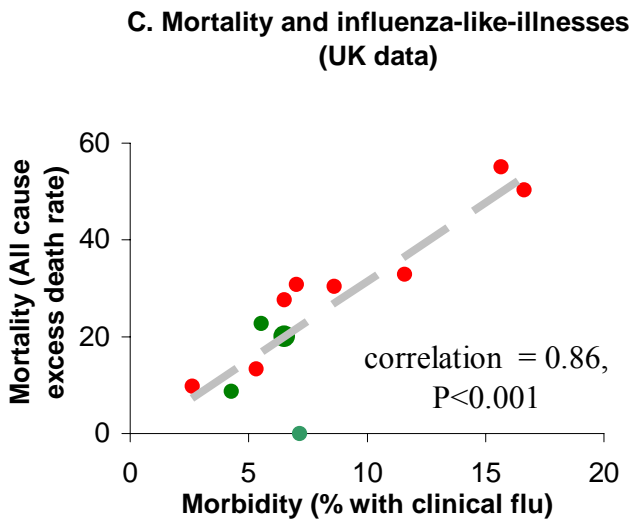
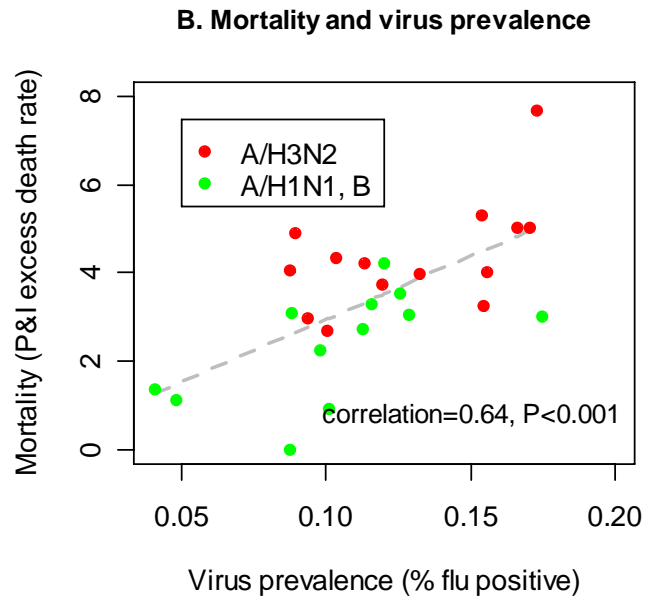
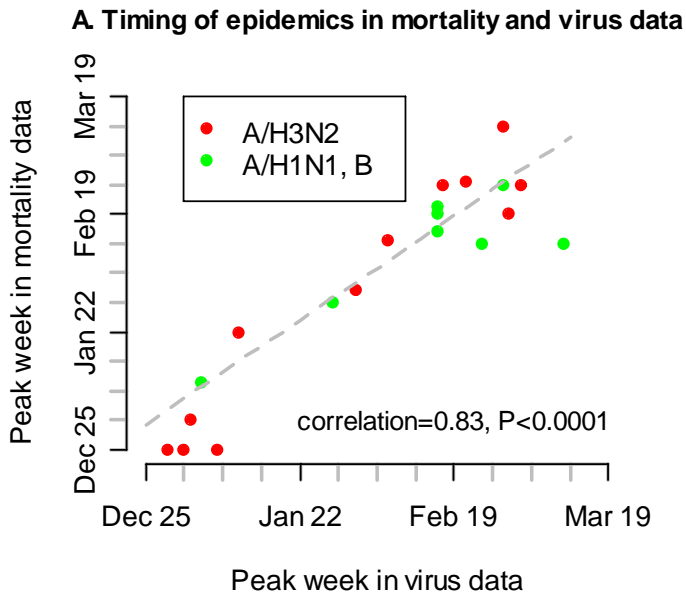
Supplementary Figure 4:

Relation between county-level workflows, population sizes and distance (gravity framework) A) Workplace = ‘recipient’ population center (B); place of residence = ‘donor’ population center.

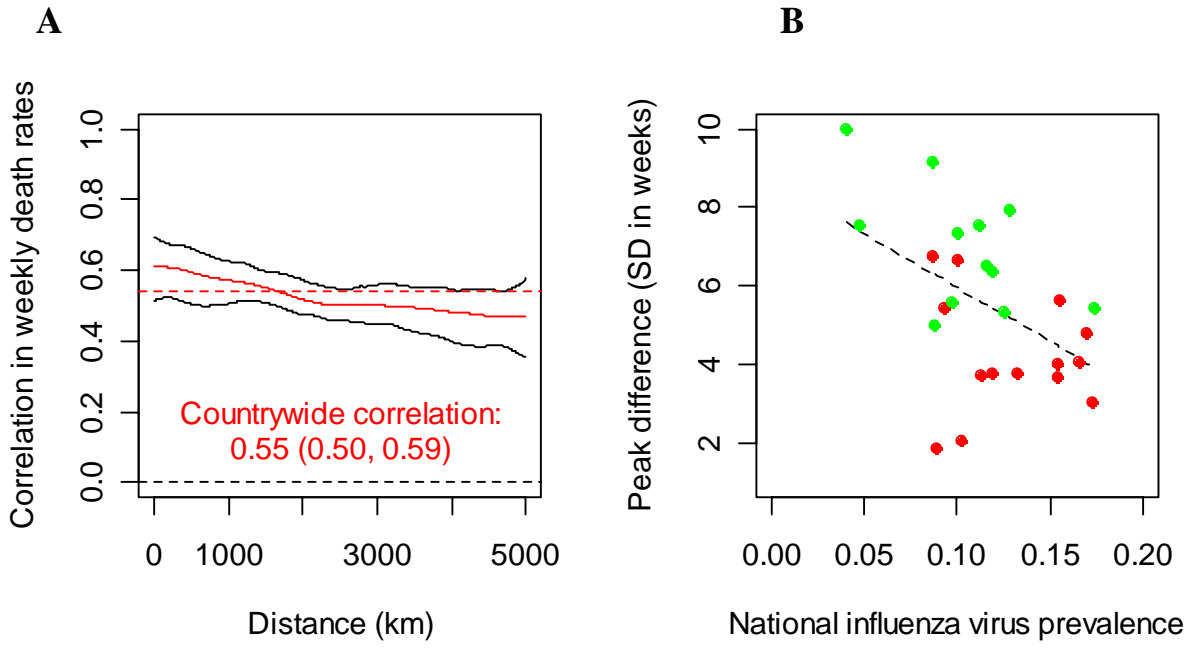
Supplementary Figure 1



Supplementary Figure 2

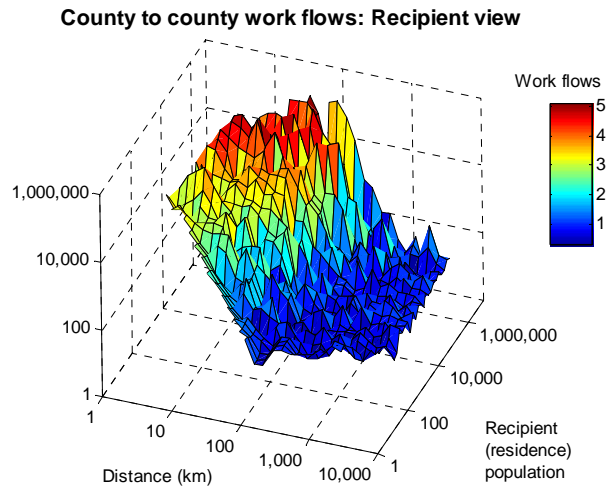


Supplementary Figure 3



Supplementary Figure 4

A)



B)

